






On Mechanisms of Proton Perpendicular Heating in the Solar Wind: Test Results Based on Wind Observations

Guo-Qing Zhao^{1,2} , Heng-Qiang Feng¹ , De-Jin Wu³ , Qiang Liu¹, Yan Zhao¹, and Zhan-Jun Tian¹

¹Institute of Space Physics, Luoyang Normal University, Luoyang 471934, China; fenghq9921@163.com

²Henan Key Laboratory of Electromagnetic Transformation and Detection, Luoyang 471934, China

³Purple Mountain Observatory, Chinese Academy of Sciences, Nanjing 210023, China

Received 2021 August 21; revised 2021 October 20; accepted 2021 October 27; published 2022 January 21

Abstract

The solar wind protons undergo significant perpendicular heating when they propagate in the interplanetary space. Stochastic heating and cyclotron resonance heating due to kinetic Alfvén waves (KAWs) are two proposed mechanisms. Which mechanism accounts for the perpendicular heating is still an open question. This paper performs tests for the two mechanisms based on Wind observations during 2004 June and 2019 May. Results show that heating rates in terms of stochastic heating theory considerably depend on the parameter of plasma β . For the solar wind with moderately high β , the theoretical heating rates are comparable to or larger than empirical heating rates, suggesting that the stochastic heating could be a powerful mechanism. For the solar wind with low β , on the contrary, the majority of data have theoretical heating rates much lower than empirical heating rates, showing that the stochastic heating seems to be weak in this case. On the other hand, it is found that, when the propagation angles of KAWs are around 70° , theoretically predicted damping wavenumbers of KAWs are equal to the observed wavenumbers at which magnetic energy spectra become significantly steep. This may imply that resonance heating due to cyclotron damping of KAWs could be another mechanism if KAWs have propagation angles around 70° .

Key words: turbulence – waves – (Sun:) solar wind

1. Introduction

It is well known that the solar wind protons undergo significant heating when they stream away from the Sun, with their temperature higher than that adiabatic theory predicts (Gazis & Lazarus 1982; Marsch et al. 1982). The isotropic adiabatic theory predicts that proton temperature decreases with the heliocentric distance and can be described by a power law r_T^n . The predicted index is $n_T = -4/3$, whereas the observed index is frequently greater than -1 for the heliocentric distance from 0.3 to 20 au. Considering that the solar wind is weakly collisional with proton distributions approximately being bi-Maxwell distribution, the double-adiabatic theory further predicts that proton perpendicular temperature reduces as r^{-2} (Chew et al. 1956; Matteini et al. 2012), while observations revealed an index around -0.9 (Hellinger et al. 2011; Perrone et al. 2019; Huang et al. 2020a). These results showed that proton perpendicular temperature decreases significantly more slowly and some perpendicular heating process must be at work in the solar wind.

On the other hand, the solar wind is commonly turbulent, and solar wind turbulence at proton scales is mainly composed of kinetic Alfvén waves (KAWs; He et al. 2012a; Klein et al. 2014; Wu & Chen 2020). Early observations first revealed that the solar wind is characterized by magnetic fluctuations over a wide scale range (Alexandrova et al. 2013; Bruno & Carbone 2013).

Fluctuations at very large scales, i.e., in the energy-containing range, are understood to be uncorrelated large-scale Alfvén waves, and have energy spectrum as $\sim f^{-1}$. Fluctuations at intermediate scales, i.e., in the inertial range, are dominated by the Kolmogorov cascade, and their energy spectrum follows a $f^{-5/3}$ law. Fluctuations at proton scales have steep spectrum with a spectral index frequently lower than the classic index $-7/3$ for dispersive cascade (Galtier 2006; Pi et al. 2020). The spectral steepening at proton scales could be attributed to turbulent dissipation and therefore heating (Leamon et al. 1998; Passot & Sulem 2015). For the nature of fluctuations at proton scales, a large body of researches based on observations and simulations showed that they are consistent with the KAW turbulence model (Bale et al. 2005; Howes et al. 2008b; Sahraoui et al. 2009, 2010; He et al. 2012b; Salem et al. 2012; Chen et al. 2013; Grošelj et al. 2018), although other models related to kinetic fast/slow magnetosonic waves are possible (Gary & Smith 2009; He et al. 2015a; Li et al. 2020). A recent statistical examination of the long-axis direction of magnetic fluctuations has also supported the KAW turbulence model (Zhao et al. 2020b).

Recent statistical analyses have shown that proton-scale KAWs appear to be relevant to proton heating in the solar wind (Zhao et al. 2020b, 2021). According to the analyses, a clear positive correlation exists between proton temperature and

magnetic energy density at proton scales. Note that the magnetic helicity favors the correlation; a higher helicity corresponds to a better correlation between the proton temperature and the magnetic energy density. Moreover, as helicity magnitude increases, the magnetic energy spectrum becomes steeper and proton temperature rises significantly (Zhao et al. 2021). In particular, the rise of the proton perpendicular temperature is faster than the parallel temperature, especially for the low- β solar wind, where β is the ratio of the plasma pressure to magnetic pressure. The magnetic helicity should be an indicator of the presence of KAWs, and the faster rise of the perpendicular temperature has been understood to be the result of the preferentially perpendicular heating by KAWs (Zhao et al. 2021). Theoretically, KAWs may heat the solar wind through stochastic heating and linearly cyclotron/Landau damping (Parashar et al. 2015; Isenberg & Vasquez 2019). The Landau damping of KAWs contributes to particle parallel heating. (Direct evidence of energy conversion from KAWs to electron parallel kinetic energy by the Landau damping was discovered in the Earth's magnetosheath (Chen et al. 2019; He et al. 2020).) For the case of protons in the solar wind, they undergo the perpendicular heating, and hence investigations on stochastic heating and cyclotron resonance heating due to KAWs will be important.

Stochastic heating is a nonlinear mechanism that may occur in the solar wind, especially when linear resonance mechanisms are suppressed (Chandran et al. 2010; Hoppock et al. 2018; Martinović et al. 2020). It arises due to the violation of magnetic moment invariance in the presence of large-amplitude turbulent fluctuations at the ion gyroscale. In this situation ions have chaotic orbits and stochastically interact with electrostatic potential as well as electromagnetic field, leading ions to diffuse toward higher energies in the direction perpendicular to the background magnetic field (Chandran et al. 2010; Hoppock et al. 2018; Martinović et al. 2020). This mechanism was first revealed by experiments in Tokamaks (McChesney et al. 1987), and later was proposed to explain the solar wind (or coronal) heating (Voitenko & Goossens 2004; Chandran et al. 2010). In particular, Chandran et al. (2010) derived an analytical expression of heating rate of stochastic heating. Using the analytical expression and Helios data, Bourouaine & Chandran (2013) carried out an observational test for the hypothesis that stochastic heating is response for the perpendicular heating in low- β solar wind streams, and Martinović et al. (2019) investigated radial evolution of stochastic heating in the low- β solar wind. Their results showed that stochastic heating likely occurs in the whole inner heliosphere. Employing Parker Solar Probe data, Martinović et al. (2020) investigated the solar wind with the heliocentric distance in the range 0.16–0.25 au and concluded that stochastic heating is possibly a dominated mechanism in the near-Sun solar wind. Nevertheless, calculations of stochastic heating rate based on Wind data at 1 au, to the best of our knowledge, are absent. Moreover, the

solar wind plasma has a wide range of β , whereas the dependence of heating rate on β has not been well discussed based on in situ data.

Cyclotron resonance heating results from cyclotron damping of Alfvén-cyclotron fluctuations, which can efficiently transfer the fluctuation energy to the particle kinetic energy in the solar wind. Theoretically, this mechanism works well for parallel propagating Alfvén-cyclotron fluctuations, often termed as ion cyclotron waves (Hollweg & Isenberg 2002; Cranmer 2014). A large number of researches supported this mechanism. The ion cyclotron wave activities have been directly observed in the solar wind (Jian et al. 2009; Zhao et al. 2018, 2019a; Woodham et al. 2019; Bowen et al. 2020; Huang et al. 2020b). The locations of the spectral break of solar wind turbulence are best associated with the prediction by the cyclotron resonance condition (Bruno & Trenchi 2014; Wang et al. 2018; Woodham et al. 2018; Duan et al. 2020). Obtained dispersion curve has a sharp transition at $kv_A/\Omega_p \sim 0.6$, which was interpreted as the ion cyclotron resonance being occurring in the solar wind (Roberts & Li 2015). Direct measures of particle kinetics as well as ion temperatures are also consistent with the cyclotron resonance heating due to ion cyclotron waves (Kasper et al. 2008, 2013; He et al. 2015b; Zhao et al. 2020a). As for very oblique Alfvén-cyclotron fluctuations (referred to as KAWs in the present paper), it has been questionable whether the cyclotron damping is effective. The solar wind turbulence is measured as anisotropic with the major populations quasi-perpendicular and is characterized by wave frequency much lower than the ion cyclotron frequency, which will weaken the cyclotron resonance interaction (Howes et al. 2008a; Sahraoui et al. 2010; He et al. 2012a; Chen et al. 2014). Nevertheless, the persistence of effective cyclotron damping of turbulent KAWs is still potentially possible according to theory (Gary & Borovsky 2004; Smith et al. 2012; Isenberg & Vasquez 2019). Further discussion on this issue should be desirable.

The purpose of this paper is to present statistical tests for the mechanisms of stochastic heating and cyclotron resonance heating according to Wind data. Particular attention will be paid to the β dependence of stochastic heating rate. For cyclotron resonance heating, this study aims to further discuss its possibility in the solar wind at 1 au. The paper is organized as follows. Existing theoretical formulae used in this paper are introduced in Section 2. The data and analysis methods are described in Section 3. Test results are displayed in Section 4. Section 5 is the summary and discussion.

2. Existing Theoretical Formulae

In order to perform tests, theoretical formulae must be employed. For stochastic heating and in the case of AW/KAW turbulence, Chandran et al. (2010) obtained an analytical formula of heating rate for a low β plasma, where the heating is

predominately due to electrostatic potential. Hoppock et al. (2018) developed the model for a plasma with moderately high β ($\beta \sim 1-30$), in which ion energization due to the solenoidal component of electric field was exploited. Consequently the expression of the total heating rate over a wide β range ($\beta \lesssim 30$) can read as follows (Hoppock et al. 2018):

$$Q_{\perp \text{stoch}} = \Omega_p v_A^2 \left[\sigma_1 \delta^3 \exp\left(-\frac{\sigma_2}{\delta}\right) + \frac{1.69c_1 \delta^3}{\beta_{\perp p}^{1/2}} \times \exp\left(-\frac{0.84c_2 \beta_{\perp p}^{1/2}}{\delta}\right) \right], \quad (1)$$

where $\delta = \delta B_{\rho}/B_0$ is the normalized magnetic-field fluctuation at the ion gyroscale, $\beta_{\perp p} = w_{\perp p}^2/v_A^2$ is the proton perpendicular beta, $w_{\perp p}$ is the proton perpendicular thermal velocity with respect to the background magnetic field, v_A is the Alfvén velocity, and $\sigma_1 = 5.0$, $\sigma_2 = 0.21$, $c_1 = 0.75$, and $c_2 = 0.34$ are constants (Chandran et al. 2010; Hoppock et al. 2018).

Empirical perpendicular heating rate is also exploited. The empirical perpendicular heating rate ($Q_{\perp \text{emp}}$) refers to the rate that is required to interpret the observed perpendicular temperature profile in the solar wind. According to the formula (Bourouaine & Chandran 2013),

$$Q_{\perp \text{emp}} = B V_p \frac{d}{dr} \left(\frac{k_B T_{\perp p}}{m_p B} \right), \quad (2)$$

and considering $T_{\perp p} \sim r^{n_T}$ and $B \sim r^{n_B}$, we rewrite $Q_{\perp \text{emp}}$ as

$$Q_{\perp \text{emp}} = (n_T - n_B) \frac{k_B T_{\perp p} V_p}{m_p r}, \quad (3)$$

where $T_{\perp p}$ is the proton perpendicular temperature, and V_p is the bulk velocity. Substituting the values $r = 1 \text{ au}$, $n_T = -0.9$, and $n_B = -1.6$ (Hellinger et al. 2011; Matteini et al. 2013; Perrone et al. 2019), Equation (3) can be further expressed as

$$Q_{\perp \text{emp}} = 3.86 \times 10^{-5} T_{\perp p} V_p \quad (\text{W kg}^{-1}), \quad (4)$$

where $T_{\perp p}$ is in units of K and V_p is in units of km s^{-1} .

For the formula concerning cyclotron resonance heating discussed in this paper, it refers to the cyclotron damping of oblique Alfvén-cyclotron fluctuations. By solving the full linear Vlasov dispersion equation, Gary & Borovsky (2004) found that (1) the proton cyclotron damping of oblique Alfvén-cyclotron fluctuations has an abrupt onset as parallel wavenumber (k_{\parallel}) increases; (2) in the regime with the proton cyclotron damping dominant, the damping rate is a weak function of the perpendicular wavenumber. For a homogeneous, isotropic, collisionless plasma, the authors fitted the damping rates of Alfvén-cyclotron fluctuations and obtained an equation to quantify the parallel wavenumber $k_{\parallel d}$, where $k_{\parallel d}$ indicates the abrupt onset of the cyclotron damping. The wavenumber $k_{\parallel d}$ depends on proton beta and can be described

as (Gary & Borovsky 2004, from their Equation 3(b))

$$k_{\parallel d} \rho_p = 0.26 \beta_p^{0.1} \quad (0.1 \leq \beta_p \leq 2). \quad (5)$$

Here, β_p is the proton beta defined by $w_{\parallel p}^2/v_A^2$ in this paper, and $w_{\parallel p}$ is the parallel thermal velocity with respect to the background magnetic field. Note that Alfvén-cyclotron fluctuations described by linear Vlasov dispersion equation become so-called KAWs when the fluctuations are obliquely propagating with respect to the background field and have perpendicular wavenumbers comparable to the proton gyroradius (Gary 1986; Zhao et al. 2014, 2016).

3. Observational Data and Analysis Methods

The data set employed in this paper is from the Wind observations between 2004 June and 2019 May. The cadence of magnetic field data is 0.092 s (Lepping et al. 1995), and the cadence of plasma data is 92 s (Ogilvie et al. 1995). The long time period of observations is divided into a series of overlapping time segments. Each time segment is set to be 200 s, and the overlap time is 100 s. The used plasma parameters include the proton density N_p , perpendicular and parallel thermal velocities $w_{\perp p}$ and $w_{\parallel p}$, and bulk velocity V_p , and are the average values over the time segment. In order to focus the study on the solar wind with negligible collision effects, only segments with small Coulomb collisional age ($A_c < 0.1$) are selected (Livi et al. 1986). In addition, it is required that the background magnetic field B_0 and bulk velocity V_p are approximately perpendicular to each other, with the angle between the both quantities in the range from 60° to 120° . This requirement first could weaken the effects of heating/cooling related to alpha-proton differential flow (Zhao et al. 2019b, 2020a). It also implies that the measured wavenumber would predominately represent the perpendicular wavenumber, which is a key parameter to describe KAWs (Hollweg 1999; Wu & Chen 2020). Finally about 3.7×10^5 time segments are satisfied.

Fast Fourier transform is conducted to obtain magnetic energy spectrum for each segment with data available. Figure 1 presents a case with the time interval 10:31:45–10:35:05 on 2005 January 1 (UT). From Figure 1(a), one can see that the spectrum has two power laws in the frequency domain, with an index approximately $-5/3$ for the lower frequency and an index about -3.6 for the higher frequency. For the frequency exceeding 3 Hz, the spectrum flattens considerably, which may result from instrument noise and/or aliasing. Proton-scale fluctuations are of interest in the present study and are described conveniently in the wavenumber domain. The wavenumber domain is from the frequency domain in terms of the Taylor frozen-in-flow hypothesis, $k = 2\pi f/V_p$ (Taylor 1938). The two vertical dotted lines in panel (a) mark the frequency range of interest. Following the study by Zhao et al. (2020b), the left vertical line denotes the wavenumber $k\rho_p = 0.1$, where $\rho_p = w_{\perp p}/\Omega_p$ and Ω_p are the proton thermal gyroradius and cyclotron frequency, respectively. The right

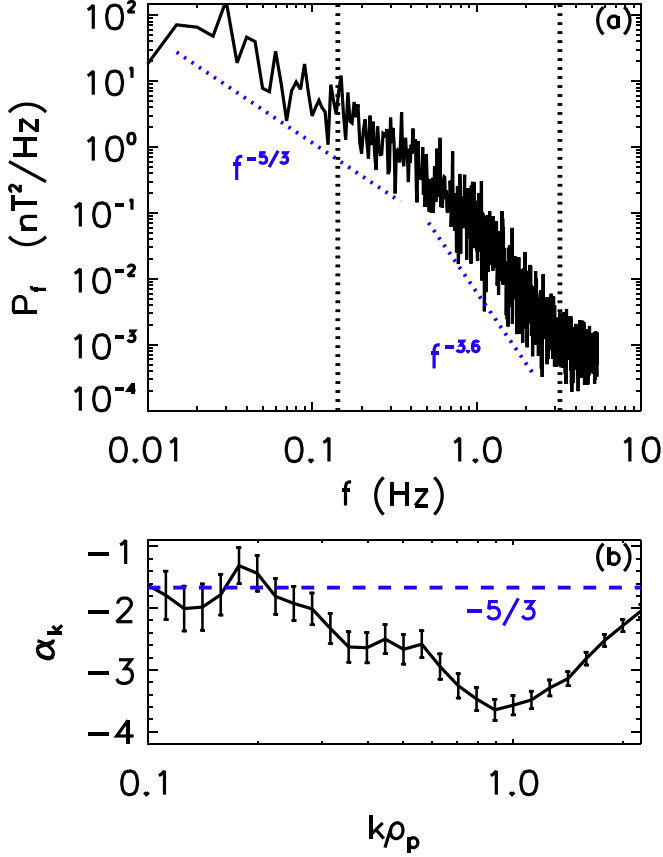


Figure 1. A case to display (a) magnetic energy spectrum P_f in the frequency domain, and (b) local spectral index α_k in the wavenumber domain. The vertical dotted lines in panel (a) mark the range shown in panel (b).

vertical line is set accordingly, requiring the spectral energy density $P_f > 10^{-3} \text{ nT}^2 \text{ Hz}^{-1}$, which could be significantly higher than the instrument noise. Panel (b) plots the local spectral index (α_k) in the wavenumber domain. The spectral index is obtained by fitting magnetic energy spectrum over the window $fe^{-0.5} \leq f \leq fe^{0.5}$. Note that for $k\rho_p < 0.3$ the spectral index is approximately around $-5/3$ (denoted by the blue horizontal dashed line), and it is more negative for $k\rho_p > 0.3$.

4. Test Results

According to the theoretical formulae and in situ data described in Sections 2 and 3, this section aims to present the test results for the two mechanisms. The test for stochastic heating is performed by calculating its heating rates and comparing them with the empirical heating rates. The test for cyclotron resonance heating is conducted by estimating the propagation angles of KAWs, at which the theoretical wavenumbers corresponding to the onset of cyclotron damping of KAWs are equal to the observed wavenumbers with magnetic energy spectra steepening.

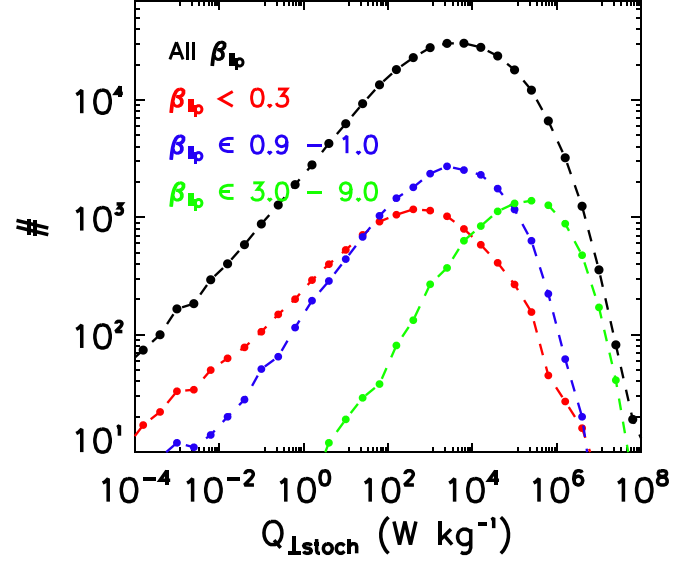


Figure 2. Distributions of stochastic heating rate $Q_{\perp\text{stoch}}$. The black, red, blue, and green lines are responsible for the cases of all $\beta_{\parallel p}$, $\beta_{\parallel p} < 0.3$, $0.9 < \beta_{\parallel p} < 1.0$, and $3.0 < \beta_{\parallel p} < 9.0$, respectively.

4.1. Stochastic Heating

Employing Equation (1) and the scheme used by Bourouaine & Chandran (2013) and Martinović et al. (2020), heating rates of stochastic heating can be calculated for the present data set. Results are plotted in Figure 2, where the black, red, blue, green lines correspond to the cases with the whole data set, subsets bounded by $\beta_{\parallel p} < 0.3$, $0.9 < \beta_{\parallel p} < 1.0$, and $3.0 < \beta_{\parallel p} < 9.0$, respectively. One can see that the heating rates span around 10 orders of magnitude and their distributions obey Gaussian distribution with tails for low heating rates, which is consistent with the results obtained by Martinović et al. (2019, 2020). Note that 43.8% of all data have heating rates greater than $5 \times 10^3 \text{ W kg}^{-1}$, implying the powerful heating ability in this population. The great heating rates support that stochastic heating likely operates in the solar wind at 1 au (Arzamasskiy et al. 2019). On the other hand, there are still 15.9% of data sharing with heating rates less than 10^2 W kg^{-1} . Such low heating rates are insufficient to heat the solar wind, which typically requires a rate of $\sim 10^3 \text{ W kg}^{-1}$ (MacBride et al. 2008; Bandyopadhyay et al. 2020). This situation is more evident in the case of low $\beta_{\parallel p}$ (red line), with the percentage of data rising up to 35.3% for the low heating rates.

It should be helpful to conduct a quantitative comparison between theoretical heating rates and empirical heating rates. Figure 3 displays such a comparison with the distribution of $Q_{\perp\text{stoch}}$ normalized by $Q_{\perp\text{emp}}$. Overall, although more data have $Q_{\perp\text{stoch}}$ up to a half of $Q_{\perp\text{emp}}$, there are still 41.0% of data with heating rate $Q_{\perp\text{stoch}} < Q_{\perp\text{emp}}/2$. (One may keep in mind that it is an unphysical result for $Q_{\perp\text{stoch}} > Q_{\perp\text{emp}}$. They are still shown in the figure just

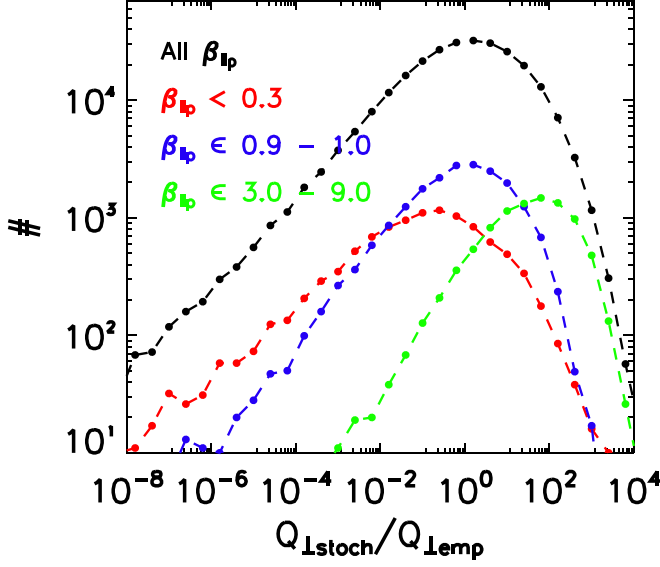


Figure 3. Distributions of stochastic heating rate $Q_{\perp\text{stoch}}$ normalized by the empirical heating rate $Q_{\perp\text{emp}}$. The black, red, blue, and green lines are responsible for the cases of all $\beta_{\parallel p}$, $\beta_{\parallel p} < 0.3$, $0.9 < \beta_{\parallel p} < 1.0$, and $3.0 < \beta_{\parallel p} < 9.0$, respectively.

for reference.) For the case of low $\beta_{\parallel p}$ (red line), the percentage is up to 67.3%. This result is in line with the recent studies by Martinović et al. (2019, 2020), who found that the radial trend of stochastic heating rates is steeper than that of empirical heating rates, and stochastic heating tends to be less significant in low- β solar wind at 1 au. As a result, additional mechanism or process beyond the stochastic heating discussed here should exist so that the measured $T_{\perp p}$ profile can be explained, at least for the population with significantly small $Q_{\perp\text{stoch}}/Q_{\perp\text{emp}}$.

In particular, results in Figures 2 and 3 imply a clear dependence of heating rates on $\beta_{\parallel p}$. The population with moderately high $\beta_{\parallel p}$ tends to have larger heating rates, which are characterized by a narrower distribution with shorter tail. On the contrary, the distribution of heating rates is wider and with longer tail for the population with low $\beta_{\parallel p}$. Figure 4(a) illustrates this dependence by plotting the distribution of $Q_{\perp\text{stoch}}/Q_{\perp\text{emp}}$ against $\beta_{\parallel p}$. This dependence corresponds the trend that the percentage of data with $Q_{\perp\text{stoch}} > Q_{\perp\text{emp}}/2$ is small for low $\beta_{\parallel p}$ and it is large for moderately high $\beta_{\parallel p}$. Figure 4(b) displays the percentage by changing $\beta_{\parallel p}$. One can see that the percentage is around 30% if $\beta_{\parallel p} < 0.4$ while it is up to nearly 100% when $\beta_{\parallel p} > 6$.

From Figures 3 and 4, $Q_{\perp\text{stoch}}$ is found to be often larger than $Q_{\perp\text{emp}}$ for $\beta_{\parallel p} \gtrsim 1$. This result seems to imply that $Q_{\perp\text{stoch}}$ is over-estimated at moderately high $\beta_{\parallel p}$. Note that $Q_{\perp\text{stoch}}$ determined by Equation (1) sensitively depends on the parameter σ_2 . With the assumption that stochastic heating alone contributes to the total heating, one can calculate σ_2 by setting $Q_{\perp\text{stoch}} = Q_{\perp\text{emp}}$ based on Equations (1) and (4).

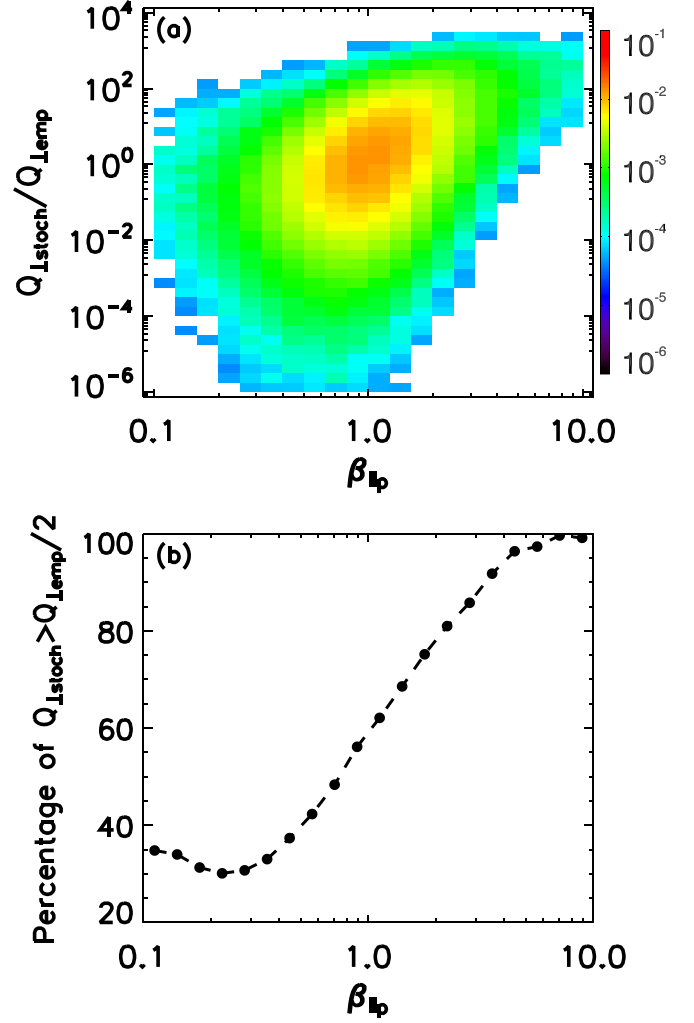


Figure 4. Panel (a) plots distribution of $Q_{\perp\text{stoch}}/Q_{\perp\text{emp}}$ against $\beta_{\parallel p}$. Panel (b) displays the percentage of data with $Q_{\perp\text{stoch}} > Q_{\perp\text{emp}}/2$ against $\beta_{\parallel p}$.

Figure 5(a) presents the result of such calculations in all $\beta_{\parallel p}$ range for the Wind data set, where the distribution of σ_2 is plotted. In calculations of σ_2 , parameters $\sigma_1 = 5.0$, $c_1 = 0.75$, and $c_2 = 0.34$ are fixed. One can see that the mean values of σ_2 , denoted by the dashed line in Figure 5(a), rapidly rise when $\beta_{\parallel p} \gtrsim 1$; they are up to 0.8 at $\beta_{\parallel p} \simeq 8$, much larger than the value of 0.21 predicted by test particle simulations with the employ of randomly phased AWs and KAWs (Hoppock et al. 2018). It is ready to understand that the larger σ_2 will result in smaller $Q_{\perp\text{stoch}}$ according to Equation (1). Similarly, one can also calculate the sensitive parameter c_2 , by setting $Q_{\perp\text{stoch}} = Q_{\perp\text{emp}}$ with fixed parameters $\sigma_1 = 5.0$, $\sigma_2 = 0.21$, and $c_1 = 0.75$. The result is displayed in Figure 5(b). One can see that the mean values of c_2 , shown by the dashed line, are smaller than the predicted value of 0.34 (Chandran et al. 2010), and are around 0.2 for $\beta_{\parallel p} < 1$. (According to our tests, $Q_{\perp\text{stoch}}$

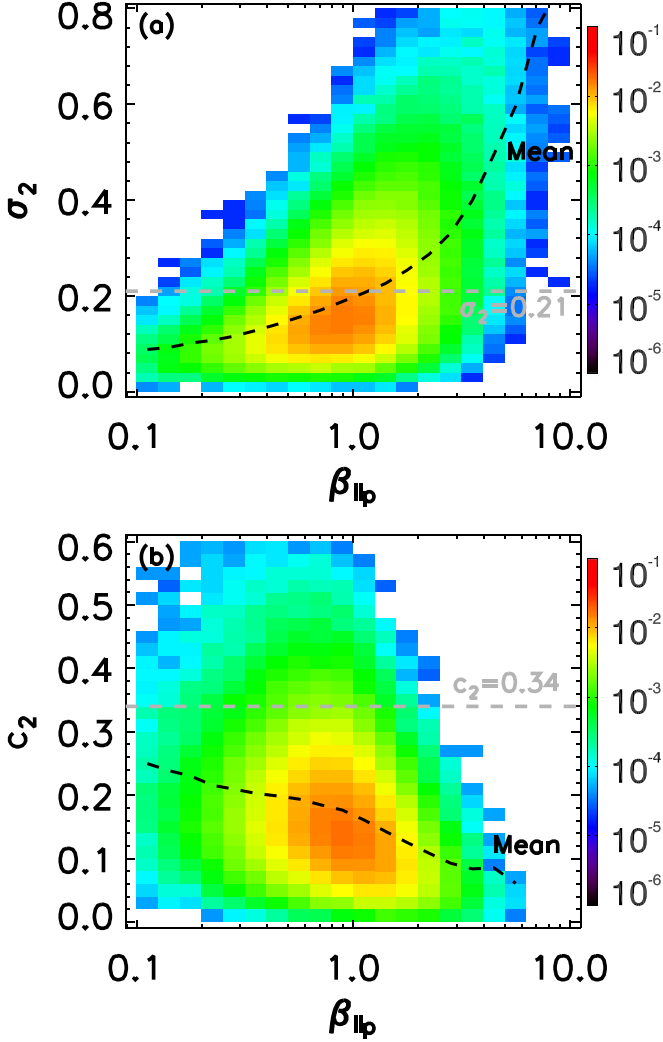


Figure 5. Panel (a) plots distribution of σ_2 that is obtained by setting $Q_{\perp\text{stoch}} = Q_{\perp\text{emp}}$ based on Equations (1) and (4), where $\sigma_1 = 5.0$, $c_1 = 0.75$, and $c_2 = 0.34$ are fixed. Panel (b) plots distribution of c_2 that is obtained similarly, where $\sigma_1 = 5.0$, $\sigma_2 = 0.21$, and $c_1 = 0.75$ are fixed. The black dashed line in (a) is responsible for mean values of σ_2 , and the black dashed line in (b) represents mean values of c_2 .

(Equation (1)) is usually dominated by the term with σ_2 for $\beta_{\parallel p} \gtrsim 1$, and by the term with c_2 for $\beta_{\parallel p} < 1$.) The smaller c_2 will contribute to larger $Q_{\perp\text{stoch}}$ based on Equation (1). Here we emphasize that the derived values of σ_2 and c_2 shown in Figure 5 are just based on the assumption of stochastic heating alone contributing to the total heating. The possible physics of this assumption and the derived values of σ_2 and c_2 need to be demonstrated, which is beyond the scope of this paper.

4.2. Cyclotron Resonance Heating

Under the assumption that the cyclotron damping of turbulent KAWs leads to spectral steepening and resonance

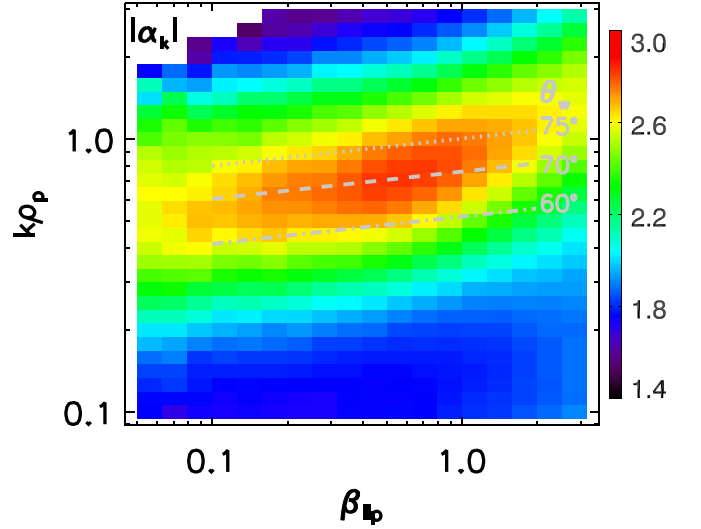


Figure 6. Color scale plot of medians of $|\alpha_k|$ in the $(\beta_{\parallel p}, k)$ space. The gray lines are the calculated wavenumbers for the onset of the cyclotron damping of KAWs with propagation angles $\theta_w = 60^\circ$, 70° , and 75° , respectively.

heating, it should be meaningful to test how much oblique for those KAWs suffering from cyclotron damping. To perform the test we first plot Figure 6 to give the distribution (medians) of observed spectral indices $|\alpha_k|$ against $(\beta_{\parallel p}, k)$, where red-yellow color indicates the region with large $|\alpha_k|$. For given KAW propagation angle θ_w and $\beta_{\parallel p}$, the wavenumber k_d ($=k_{\parallel d}/\cos(\theta_w)$), corresponding to the abrupt onset of the cyclotron damping of KAWs, is a function of θ_w and can be calculated in terms of Equation (5). The calculated k_d is displayed by three gray lines for $\theta_w = 60^\circ$, 70° , and 75° , respectively, in Figure 6. It is interesting that the lines with these θ_w overlap on the region with large $|\alpha_k|$. This result implies that KAWs with $\theta_w \lesssim 75^\circ$ could be dissipated by cyclotron damping and the damping of KAWs with $60^\circ \lesssim \theta_w \lesssim 75^\circ$ may result in the steeper magnetic spectra. (On the other hand, the observed KAWs in the solar wind might be merely the remains of KAWs that have larger propagation angles and suffer from little damping.) Note that the upper limit of 75° could be slightly higher if KAWs are propagating obliquely to the flow direction of the solar wind. In that case only the finite component of the wavevector is measured and larger wavenumber can be expected, which favors the damping.

It should be noted that the test here is performed by comparing the abrupt onset position of cyclotron damping with the largest $|\alpha_k|$ corresponding to the steepest spectral range. This is different from previous works, in which the wavenumber of cyclotron resonance is usually compared with the spectral break (e.g., Bruno & Telloni 2015; Duan et al. 2018; Wang et al. 2018; Woodham et al. 2018). The wavenumber of cyclotron resonance in previous works was

derived from the cyclotron resonance condition (Leamon et al. 1998), while the wavenumber used in this paper was obtained by solving the full linear Vlasov dispersion equation and fitting the damping rates of Alfvén-cyclotron fluctuations (Gary & Borovsky 2004).

5. Summary and Discussion

Previous studies have shown that the solar wind proton heating frequently occurs in the direction perpendicular to the ambient field (Gazis & Lazarus 1982; Marsch et al. 1982; Perrone et al. 2019; Huang et al. 2020a). Our recent statistical analyses confirmed the preferentially perpendicular heating with $\beta_{\parallel p} \lesssim 1$ (Zhao et al. 2020b, 2021). On the other hand, a large body of existing research has demonstrated that the solar wind turbulence at proton scales is dominated by KAWs (He et al. 2012b; Podesta 2013; Grošelj et al. 2018; Wu & Chen 2020). Two mechanisms including stochastic heating and cyclotron resonance heating due to KAWs are thus relevant. Based on 15 yr of Wind observations, this paper has carried out statistical tests on both mechanisms.

The first test is to investigate the theoretical heating rates in terms of stochastic heating due to large-amplitude AW/KAW fluctuations, and compare them with empirical heating rates that are required to explain the measured $T_{\perp p}$ profile in the solar wind. Results show that theoretical heating rates considerably depend on the parameter $\beta_{\parallel p}$. For moderately high $\beta_{\parallel p}$, theoretical heating rates are comparable to or larger than empirical heating rates, suggesting the stochastic heating as a powerful heating mechanism. For low $\beta_{\parallel p}$ ($\beta_{\parallel p} < 0.3$), about 67% of the data have heating rates less than half of the empirical heating rates, showing that the stochastic heating alone seems unable to complete the heating required to explain the measured $T_{\perp p}$ profile. This result tends to indicate that additional mechanism or process should arise, at least in case of the low- $\beta_{\parallel p}$ solar wind. With this regard, other mechanisms, such as cyclotron resonance heating and/or intermittent effects (Xia et al. 2013; Mallet et al. 2019), should be further exploited.

The second test is to estimate the propagation angles of KAWs, at which the theoretically predicted damping wavenumbers are approximately equal to the observed wavenumbers with significantly steepening of magnetic energy spectra. It is found that the angles are around 70° , with the upper limit of 75° or slightly larger. An implication of this test is that the cyclotron damping of KAWs with propagation angles around 70° may occur and (partly) account for the steepening of the spectra. It might also mean that KAWs with propagation angles not sufficiently large ($\lesssim 75^\circ$) would be significantly weaker than those KAWs with large propagation angles ($> 80^\circ$) in the solar wind, when one considers that the cyclotron resonance is efficient to rapidly remove the wave energy of KAWs with smaller propagation angles. In addition, for KAWs with large




propagation angles ($> 80^\circ$), they may also experience net damping during their propagation process because the solar wind is inherently turbulent. The directions of the ambient field, and therefore propagation angles of KAWs, should vary considerably in space and time.

In summary, this paper performs statistical tests on two mechanisms relevant to proton perpendicular heating based on in situ observations at 1 au. It is particularly shown that stochastic heating rates considerably depend on the plasma $\beta_{\parallel p}$; the stochastic heating could appear as a powerful mechanism for the solar wind with moderately high $\beta_{\parallel p}$, while it seems to be weak in the solar wind with low $\beta_{\parallel p}$. On the other hand, heating due to cyclotron damping of KAWs could be another mechanism if KAWs have propagation angles around 70° , which may account for the steepening of magnetic energy spectra of the low- $\beta_{\parallel p}$ solar wind. These results should be helpful to discuss the issue of turbulent dissipation and heating in the solar wind. We remark that the present study is preliminary and further research with simulations should be desirable in the future.

Acknowledgments

This research was supported by the National Natural Science Foundation of China under grant Nos. 41874204, 41974197 and 11873018. Research by G.-Q. Zhao was supported partly by the Project for Scientific Innovation Talent in Universities of Henan Province (19HASTIT020). The authors acknowledge the Wind mission for the data, which can be obtained via the Coordinated Data Analysis Web (http://cdaweb.gsfc.nasa.gov/cdaweb/istp_public/). The authors also thank the referee for helpful comments that improved this paper.

ORCID iDs

Guo-Qing Zhao  <https://orcid.org/0000-0002-1831-1451>
 Heng-Qiang Feng  <https://orcid.org/0000-0003-2632-8066>
 De-Jin Wu  <https://orcid.org/0000-0003-2418-5508>

References

- Alexandrova, O., Chen, C. H. K., Sorriso-Valvo, L., Horbury, T. S., & Bale, S. D. 2013, *SSRv*, **178**, 101
- Arzamasskiy, L., Kunz, M. W., Chandran, B. D. G., & Quataert, E. 2019, *ApJ*, **879**, 53
- Bale, S. D., Kellogg, P. J., Mozer, F. S., Horbury, T. S., & Reme, H. 2005, *PhRvL*, **94**, 215002
- Bandyopadhyay, R., Goldstein, M. L., Maruca, B. A., et al. 2020, *ApJS*, **246**, 48
- Bourouaine, S., & Chandran, B. D. G. 2013, *ApJ*, **774**, 96
- Bowen, T. A., Mallet, A., Huang, J., et al. 2020, *ApJS*, **246**, 66
- Bruno, R., & Carbone, V. 2013, *LRSP*, **10**, 2
- Bruno, R., & Telloni, D. 2015, *ApJL*, **811**, L17
- Bruno, R., & Trenchi, L. 2014, *ApJL*, **787**, L24
- Chandran, B. D. G., Li, B., Rogers, B. N., Quataert, E., & Germaschewski, K. 2010, *ApJ*, **720**, 503
- Chen, C. H. K., Boldyrev, S., Xia, Q., & Perez, J. C. 2013, *PhRvL*, **110**, 225002
- Chen, C. H. K., Klein, K. G., & Howes, G. G. 2019, *NatCo*, **10**, 740

- Chen, C. H. K., Leung, L., Boldyrev, S., Maruca, B. A., & Bale, S. D. 2014, *GeoRL*, **41**, 8081
- Chew, G. F., Goldberger, M. L., & Low, F. E. 1956, *RSPSA*, **236**, 112
- Cranmer, S. R. 2014, *ApJS*, **213**, 16
- Duan, D., Bowen, T. A., Chen, C. H. K., et al. 2020, *ApJS*, **246**, 55
- Duan, D., He, J., Pei, Z., et al. 2018, *ApJ*, **865**, 89
- Galtier, S. 2006, *JPIPh*, **72**, 721
- Gary, S. P. 1986, *JPIPh*, **35**, 431
- Gary, S. P., & Borovsky, J. E. 2004, *JGRA*, **109**, A06105
- Gary, S. P., & Smith, C. W. 2009, *JGRA*, **114**, A12105
- Gazis, P. R., & Lazarus, A. J. 1982, *GeoRL*, **9**, 431
- Grošelj, D., Mallet, A., Loureiro, N. F., & Jenko, F. 2018, *PhRvL*, **120**, 105101
- He, J., Tu, C., Marsch, E., & Yao, S. 2012a, *ApJ*, **749**, 86
- He, J., Tu, C., Marsch, E., & Yao, S. 2012b, *ApJL*, **745**, L8
- He, J., Tu, C., Marsch, E., et al. 2015a, *ApJL*, **813**, L30
- He, J., Wang, L., Tu, C., Marsch, E., & Zong, Q. 2015b, *ApJL*, **800**, L31
- He, J., Zhu, X., Verscharen, D., et al. 2020, *ApJ*, **898**, 43
- Hellinger, P., Matteini, L., Štverák, Š., Trávníček, P. M., & Marsch, E. 2011, *JGRA*, **116**, A09105
- Hollweg, J. V. 1999, *JGR*, **104**, 14811
- Hollweg, J. V., & Isenberg, P. A. 2002, *JGRA*, **107**, 1147
- Hoppock, I. W., Chandran, B. D. G., Klein, K. G., Mallet, A., & Verscharen, D. 2018, *JPIPh*, **84**, 905840615
- Howes, G. G., Cowley, S. C., Dorland, W., et al. 2008a, *JGRA*, **113**, A05103
- Howes, G. G., Dorland, W., Cowley, S. C., et al. 2008b, *PhRvL*, **100**, 065004
- Huang, J., Kasper, J. C., Vech, D., et al. 2020a, *ApJS*, **246**, 70
- Huang, S. Y., Zhang, J., Sahraoui, F., et al. 2020b, *ApJL*, **897**, L3
- Isenberg, P. A., & Vasquez, B. J. 2019, *ApJ*, **887**, 63
- Jian, L. K., Russell, C. T., Luhmann, J. G., et al. 2009, *ApJL*, **701**, L105
- Kasper, J. C., Lazarus, A. J., & Gary, S. P. 2008, *PhRvL*, **101**, 261103
- Kasper, J. C., Maruca, B. A., Stevens, M. L., & Zaslavsky, A. 2013, *PhRvL*, **110**, 091102
- Klein, K. G., Howes, G. G., TenBarge, J. M., & Podesta, J. J. 2014, *ApJ*, **785**, 138
- Leamon, R. J., Smith, C. W., Ness, N. F., Matthaeus, W. H., & Wong, H. K. 1998, *JGR*, **103**, 4775
- Lepping, R. P., Acuña, M. H., Burlaga, L. F., et al. 1995, *SSRv*, **71**, 207
- Li, H., Li, N., Wang, C., & Yao, S. 2020, *ApJL*, **889**, L16
- Livi, S., Marsch, E., & Rosenbauer, H. 1986, *JGR*, **91**, 8045
- MacBride, B. T., Smith, C. W., & Forman, M. A. 2008, *ApJ*, **679**, 1644
- Mallet, A., Klein, K. G., Chandran, B. D. G., et al. 2019, *JPIPh*, **85**, 175850302
- Marsch, E., Schwenn, R., Rosenbauer, H., et al. 1982, *JGR*, **87**, 52
- Martinović, M. M., Klein, K. G., & Bourouaine, S. 2019, *ApJ*, **879**, 43
- Martinović, M. M., Klein, K. G., Kasper, J. C., et al. 2020, *ApJS*, **246**, 30
- Matteini, L., Hellinger, P., Goldstein, B. E., et al. 2013, *JGRA*, **118**, 2771
- Matteini, L., Hellinger, P., Landi, S., Trávníček, P. M., & Velli, M. 2012, *SSRv*, **172**, 373
- McChesney, J. M., Stern, R. A., & Bellan, P. M. 1987, *PhRvL*, **59**, 1436
- Ogilvie, K. W., Chornay, D. J., Fritzenreiter, R. J., et al. 1995, *SSRv*, **71**, 55
- Parashar, T. N., Salem, C., Wicks, R. T., et al. 2015, *JPIPh*, **81**, 905810513
- Passot, T., & Sulem, P. L. 2015, *ApJL*, **812**, L37
- Perrone, D., Stansby, D., Horbury, T. S., & Matteini, L. 2019, *MNRAS*, **483**, 3730
- Pi, G., Pitňa, A., Němeček, Z., et al. 2020, *SoPh*, **295**, 84
- Podesta, J. J. 2013, *SoPh*, **286**, 529
- Roberts, O. W., & Li, X. 2015, *ApJ*, **802**, 1
- Sahraoui, F., Goldstein, M. L., Belmont, G., Canu, P., & Rezeau, L. 2010, *PhRvL*, **105**, 131101
- Sahraoui, F., Goldstein, M. L., Robert, P., & Khotyaintsev, Y. V. 2009, *PhRvL*, **102**, 231102
- Salem, C. S., Howes, G. G., Sundkvist, D., et al. 2012, *ApJL*, **745**, L9
- Smith, C. W., Vasquez, B. J., & Hollweg, J. V. 2012, *ApJ*, **745**, 8
- Taylor, G. I. 1938, *RSPSA*, **164**, 476
- Voitenko, Y., & Goossens, M. 2004, *ApJL*, **605**, L149
- Wang, X., Tu, C., He, J., & Wang, L. 2018, *ApJ*, **857**, 136
- Woodham, L. D., Wicks, R. T., Verscharen, D., et al. 2019, *ApJL*, **884**, L53
- Woodham, L. D., Wicks, R. T., Verscharen, D., & Owen, C. J. 2018, *ApJ*, **856**, 49
- Wu, D. J., & Chen, L. 2020, *Kinetic Alfvén Waves in Laboratory, Space, and Astrophysical Plasmas* (Singapore: Springer)
- Xia, Q., Perez, J. C., Chandran, B. D. G., & Quataert, E. 2013, *ApJ*, **776**, 90
- Zhao, G. Q., Feng, H. Q., Wu, D. J., et al. 2018, *JGRA*, **123**, 1715
- Zhao, G. Q., Feng, H. Q., Wu, D. J., Pi, G., & Huang, J. 2019a, *ApJ*, **871**, 175
- Zhao, G. Q., Feng, H. Q., Wu, D. J., et al. 2020a, *ApJL*, **889**, L14
- Zhao, G. Q., Li, H., Feng, H. Q., et al. 2019b, *ApJ*, **884**, 60
- Zhao, G. Q., Lin, Y., Wang, X. Y., et al. 2020b, *GeoRL*, **47**, e89720
- Zhao, G. Q., Lin, Y., Wang, X. Y., et al. 2021, *ApJ*, **906**, 123
- Zhao, J. S., Voitenko, Y., Yu, M. Y., Lu, J. Y., & Wu, D. J. 2014, *ApJ*, **793**, 107
- Zhao, J. S., Voitenko, Y. M., Wu, D. J., & Yu, M. Y. 2016, *JGRA*, **121**, 5